Far-infrared spectra of indium selenide single crystals

C. Julien, M. Eddrief, and M. Balkanski
Laboratoire de Physique des Solides, Université Pierre et Marie Curie, 4 place Jussieu, 75252 Paris CEDEX 05, France

A. Chevy
Laboratoire de Physique des Milieux Condensés, Université Pierre et Marie Curie, 4 place Jussieu, 75252 Paris CEDEX 05, France
(Received 21 October 1991; revised manuscript received 24 February 1992)

Far-infrared spectra of different indium selenide compounds are reported. Both polarizations $\mathbf{E}\perp c$ and $\mathbf{E}\parallel c$ have been recorded in the layered materials InSe,In_2Se_3, In_4Se_3, and $InSe_{1.2}$ crystals. Analyses of the reflection spectra are made by application of the Kramers-Kronig relationship and a Lorentzian oscillator fitting. Accurate values for the frequencies and oscillator strengths of the infrared-active modes have been obtained. The temperature dependences of the frequency and lifetime of the phonon in InSe are investigated using the anharmonic model with two- and three-phonon decay function. Far-infrared spectra of doped layered materials and lithium-intercalated In_2Se_3 are also presented. Vibrational and electronic properties are discussed. Free-carrier data are deduced from the optical measurements using a single-particle Drude model and compared with those obtained by Hall-effect measurements.

I. INTRODUCTION

Layered structures that contain highly anisotropic physical properties are formed by atoms strongly bounded by covalent or ionic forces within the layer while individual layers are held together by relatively a much weaker force. The latter is frequently referred to as the van der Waals interaction, though contributions from covalent and ionic interactions are also encountered, particularly in the intercalation complexes.[1] Graphite is the prototype lamellar crystal, and layered structures include the well-known transition-metal dichalcogenides, various metal dihalides, trihalides, or oxyhalides.[2] They are rather attractive because they present many original physical properties that are not commonly encountered in the three-dimensional materials. III-VI compounds such as gallium selenide, gallium sulfide, or indium selenide belong to this class of layered structures, and their interest originates from their potential usefulness in semiconducting devices.[3,4]

The In-Se phase diagram, which has been reported by Slavnova and Eliseev[5] and, more recently by Likforman and Guittard,[6] indicated that four compounds exist, In_4Se_3, InSe, $InSe_{1.2}$, and In_2Se_3. Among these compounds, InSe, which has a band gap of 1.29 eV at room temperature, is the most studied and has the simplest crystallographic structure. In_2Se_3 is also a semiconductor which exhibits a number of structural modifications and complicated low-temperature phase. Three phases have been detected:[7] α-In_2Se_3 is stable at room temperature ($E_g=1.356$ eV), β-In_2Se_3 is formed above 473 K ($E_g=1.308$ eV), and γ-In_2Se_3 is the phase obtained above 623 K with $E_g=1.812$ eV. Recent investigations of electrical and optical properties of In_2Se_3 with respect to the post preparation annealing treatment show that the disorder in this layered material decreases as the two-dimensional (2D) character is more pronounced.[8,9] In_4Se_3 is a semiconductor with $E_g=0.82$ eV (Ref. 10) which exhibits a high electrical conductivity of 1 $\Omega^{-1}\,\mathrm{cm}^{-1}$ at room temperature. Its structure is composed of endless interlocking chains running parallel to the c axis. $InSe_{1.2}$ or In_5Se_6 is a monoclinic crystal which appears in the form of thin needles along the b axis. This compound exhibits a semiconducting character with $E_g=0.31$ eV and a conductivity of 0.01 $\Omega^{-1}\,\mathrm{cm}^{-1}$ at room temperature.[11]

In this paper we report spectra of the first-order phonon excitation of the indium selenide single crystals determined by long-wavelength infrared spectroscopy. Values for the frequencies and oscillator strengths of the infrared-active phonons have been obtained. Far-infrared spectra of doped layered materials and lithium-intercalated In_2Se_3 are also presented. Vibrational and electronic properties and their modification upon lithium intercalation are discussed.

II. EXPERIMENT

Let us introduce first the characteristics of the different indium selenide samples studied here. Crystallographic data, including crystal symmetry and unit-cell parameters of the compounds in the system In-Se, are listed in Table I. InSe is made of a fourfold stacking of Se-In-In-Se sheets which characterizes all M_2X_2 molecular-like crystals. The Bridgman grown crystals usually belong to the γ modification;[12,13] their unit cell is rhombohedral and contains one molecular unit per three layer.[14] Samples are cleaved from the Bridgman ingot and have a resistivity of 3.1 Ω cm, a concentration of n-type carriers of 8.6×10^{15} cm^{-3}, and a Hall mobility of 230 $\mathrm{cm}^2\,\mathrm{V}^{-1}\,\mathrm{s}^{-1}$ at room temperature. In_2Se_3 is an n-type semiconductor and the α phase is layered and contains hexagonal alternating sheets forming the sequence Se-In-Se-In-Se which are packed hexagonally as viewed along

 ©1992 The American Physical Society

TABLE I. Crystallographic data of In-Se systems.

Compound	Crystal symmetry	Unit-cell parameters (nm)
InSe[a]	Rhombohedral	$a=0.4002$
	$R3m$	$c=0.875$
In_2Se_3[b]	Hexagonal	$a=0.402$
	$P6_3/mmc$	$c=1.923$
In_4Se_3[c]	Orthorhombic	$a=1.5297$
	$P2/m$	$b=1.2308$
		$c=0.4081$
In_5Se_6[d]	Monoclinic	$a=1.765$
	$P2/m$	$b=0.409$
		$c=0.945$
		$\beta=101.10$

[a]Reference 6.
[b]Reference 13.
[c]Reference 16.
[d]Reference 17.

the c axis with a weak bonding between the Se-Se layers separated by a distance of 0.307 nm forming the van der Waals space.[15] Samples of In_2Se_3 have been prepared by direct fusion of elements and annealed at 453 K over periods from a few hours to a week in order to obtain electrical conductivity of 0.06 $\Omega^{-1}\,cm^{-1}$, carrier concentration of 5×10^{16} cm^{-3}, and Hall mobility of 8.2 $cm^2\,V^{-1}\,s^{-1}$.[14] $InSe_{1.2}$ and In_4Se_3 have been prepared by direct fusion of elements in a sealed evacuated tube held at 700 °C for several hours. $InSe_{1.2}$ crystal which is formed by black needles has a rather complex structure[16–18] which consists of two separate sections of almost cubic close-packed arrays of Se atoms with In atoms in octahedral coordination and a unit cell containing 26 atoms. In_4Se_3 is the higher conducting semiconductor of the binary In-Se system. The structure is orthorhombic space group *Pnnm* with 28 atoms per unit cell. Samples of InSe and In_2Se_3 have been cleaved to obtain a surface with good optical quality. Measurements of In_4Se_3 and $InSe_{1.2}$ have been determined for a mosaic sample composed of oriented single-crystal plates whose surfaces formed a natural cleavage face.

Far-infrared (FIR) spectra are recorded on a Bruker IFS 113 vacuum Fourier-transform interferometer. Samples are placed under vacuum in a variable-temperature Oxford (model CF 1104) cryostat. A liquid-helium bolometer is used as detector, and each spectrum is the average of 100 fast scans with a spectral resolution of 1 cm^{-1}. Reflectivity measurements are carried out using a quasispecular reflection unit working at incidence angle of 11° and allowing the spectrum to be obtained on small samples of 2 mm diameter.

III. RESULTS AND DISCUSSION

A. Phonon spectra of In-Se crystals at room temperature

1. InSe

Figure 1 shows the reflectivity spectra of γ-InSe at room temperature for polarizations $\mathbf{E}\perp c$ (*s*-polarized light) (curve *a*) and $\mathbf{E}\parallel c$ (*p*-polarized light) (curve *b*). Only one dominant reststrahl band is found in each polarization in agreement with the prediction of group theory.[19] The main feature is associated with the E_{1u} mode ($\mathbf{E}\perp c$) and the A_{2u} mode ($\mathbf{E}\parallel c$). Both a Kramers-Kronig and a Lorentzian-oscillator dispersion analysis are performed. A first approximation for the oscillator parameter is obtained by Kramers-Kronig fitting and used in the fit of the reflectance spectrum which is carried out using the model of independent oscillators.[20]

The reflectivity factor R is related to the dielectric constant through the Fresnel equation

$$R=\{[\epsilon(\omega)^{1/2}-1]/[\epsilon(\omega)^{1/2}+1]\}^2 . \quad (1)$$

The general form of the complex dielectric function $\epsilon(\omega)=\epsilon_1+i\epsilon_2$ can be written

$$\epsilon(\omega)=\epsilon_\infty+\sum_i \epsilon_{\rm ph}+\sum_j \epsilon_{\rm FC} , \quad (2)$$

where ϵ_∞ is the high-frequency dielectric constant, $\epsilon_{\rm Ph}$ is the complex dielectric term due to photons, and $\epsilon_{\rm FC}$ is the complex dielectric term due to free carriers, as defined by the Drude formalism. At finite temperature, Eq. (2) can then be written as a set of separate equation for the real and imaginary parts of a wave-number-dependent dielectric function

$$\epsilon(\omega)=\epsilon_\infty+\sum_i \frac{4\pi f_i\omega_{T,i}^2}{\omega_{T,i}^2-\omega^2-i\omega\gamma_i}-\sum_j \frac{\epsilon_\infty\omega_{p,j}^2}{\omega^2-i\omega\gamma_{p,j}} , \quad (3)$$

where $\omega_{T,i}$ is the resonance frequency of the ith lattice oscillator and γ_i is the lattice damping factor at the ith lattice oscillator; f_i is the oscillator strength for the ith oscillator with $f_i=(\epsilon_0-\epsilon_\infty)$. The plasma resonance frequency $\omega_{p,j}$ is defined by

$$\omega_{p,j}=(4\pi N_j e^2/m^*\epsilon_\infty)^{1/2} , \quad (4)$$

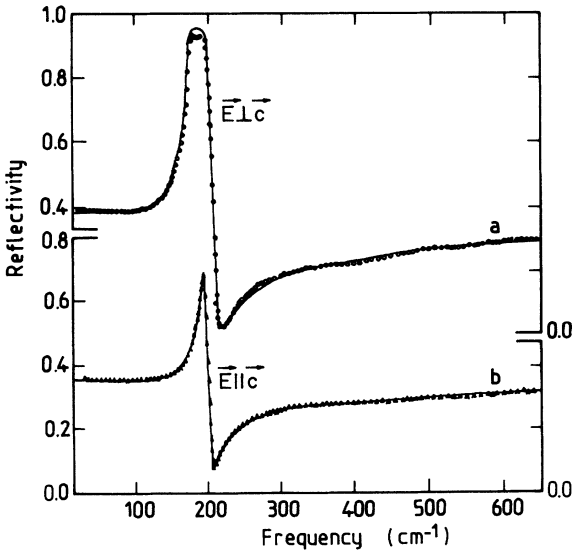

FIG. 1. Far-infrared reflectivity spectra of γ-InSe single crystal recorded at room temperature with incident light polarization $\mathbf{E}\perp c$ (curve *a*) and $\mathbf{E}\parallel c$ (curve *b*). Dots are experimental data and full line is the best fit using Eq. (3).

where N_j is the free-carrier concentration and m^* is the free-carrier effective mass, and $\gamma_{p,j}$ is the plasma damping parameter.

Using Eqs. (1) and (3) for the study of InSe where the free-carrier contribution is not included, the least-squares fitting is performed on the measured reflectivity. The parameters used in these calculations are collected in Table II, together with the available data of the literature[21–23] given for comparison. We notice that the E_{1u} mode has an oscillator strength parameter $S_{1u}=2\pi f_{1u}$ which is 35 times larger than the A_{2u} mode characterizing the strong anisotropy of InSe. These result are in good agreement and assignment of the modes is in good accordance with the data obtained by Raman scattering measurements.[14] In order to make the results more consistent we use the least-squares technique to determine dielectric constants ϵ_0 and ϵ_∞ which together with the experimentally determined values of transverse optical (TO) and longitudinal optical (LO) phonons satisfy the Lyddane-Sachs-Teller relation.[24] Thus the oscillator energy can be calculated from the imaginary part of the complex dielectric function[25] by the expression

$$p_i=\epsilon''_{\max}\Gamma_{T,i}\omega_{T,i} \ . \tag{5}$$

Values of 112 710 and 21 531 cm^{-2} are found for $p_\perp$ and $p_\parallel$, respectively, in γ-InSe.

Figure 2 shows the far-infrared transmittance spectra of a thin slab of γ-InSe at different temperatures between 5 and 300 K. These measurements have been carried out in the polarization E$\perp c$. The transmittance spectrum exhibits an intense absorption band at 180 cm^{-1} at room temperature. This spectral line shape is typical of the single reststrahlen band of a thin polar crystal. The best fit to the spectrum in terms of the single oscillator model is obtained with the frequency of $\omega_{TO}=176$ cm^{-1} for the transverse optical mode with a strong oscillator strength. The extrapolation of transmittance to 100% gives the frequency of the LO phonon at 214 cm^{-1}. From the fit, static and high-frequency dielectric constants of 12.3 and 8.3, respectively, are calculated. The frequencies agree well with these obtained by reflectivity measurements.

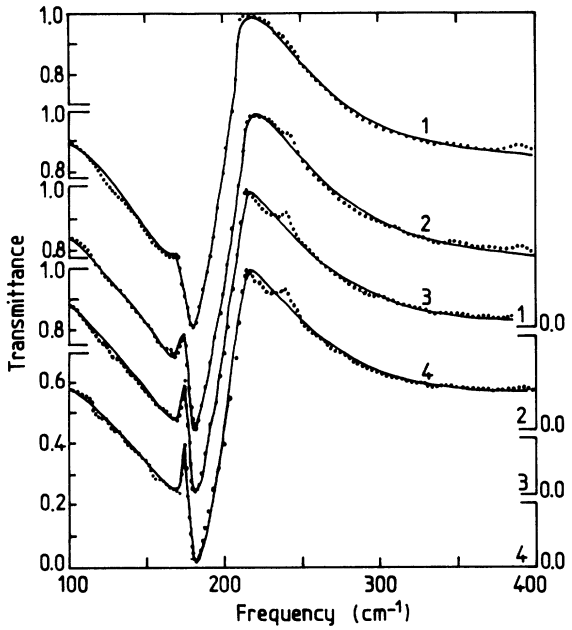

FIG. 2. Far-infrared transmittance spectra of γ-InSe single crystal at different temperatures (1) 300 K; (2) 200 K; (3) 100 K; (4) 5 K. These spectra are recorded for the polarization E$\perp c$.

The transverse effective charge e_T^* is given by[25]

$$e_T^*=[M\epsilon_\infty/4\pi ne^2(\omega_{LO}^2-\omega_{TO}^2)]^{1/2} \ , \tag{6}$$

where n is the number of anion-cation pairs per unit volume and M is the reduced mass of the considered pair. Substituting experimental parameters obtained by the present transmittance measurements into Eq. (6) and taking $n=1.7\times10^{22}$ cm^{-3}, we obtain $e^*_{T(\perp)}=2.49$ and $e^*_{T(\parallel)}=0.45$. We can remark (i) the effect of the anisotropy on the effective charge in InSe, (ii) the effective charge for the in-plane mode is higher than that along the c axis and, (iii) the ratio $e_T^*(\perp)/e_T^*(\parallel)$ is 5.53 in InSe. This may be taken as evidence from the strongest ionicity in InSe. These values can be compared to those of the transition-metal dichalcogenides. The smallest value ($e_T^*/e=0.6$)

TABLE II. Mode parameters and literature data.

	Modes						
	E_{1u}(E$\perp c$)		A_{2u}(E$\parallel c$)				
	ω_{TO} (cm^{-1})	ω_{LO} (cm^{-1})	ω_{TO} (cm^{-1})	ω_{LO} (cm^{-1})	$\gamma_{\perp,\parallel}$ (cm^{-1})	$S_{\perp,\parallel}$	$\epsilon_{\infty\perp,\parallel}$
a	178	212	190	199	4.2	3.5	8.5
					0.9	0.1	6.15
b	173	205	191	199	3.6	3.1	8.8
					1.0	0.7	7.8
c	178	210	189	198			6.2
						4.9	
d	178	214	202	203	5.3	4.0	8.5
					0.09	8.0	

[a]This work.
[b]Reference 21.
[c]Reference 22.
[d]Reference 23.

in MoS_2 which has a covalent character and the highest ($e_T^*/e=4.4$) in ZrS_2 which is ioniclike have been determined. Nevertheless, as pointed out by Lucovsky *et al.*,[26] the relatively high values of e_T^*/e for the III-VI compounds imply that the chemical bonding is covalent. This is due to the charge transfer from the Se atoms to the In atoms; here each In atom makes four bonds but has only three electrons.

When the temperature decreases, the frequency of the reststrahlen band increases as expected in the classical theory (from 181.4 cm^{-1} at 300 K to 182.6 cm^{-1} at 5 K). Two other peaks are situated at 176 and 239 cm^{-1} at lower temperature. The peak at 239 cm^{-1} is attributed to the combination $A_{2u}(LO)+E_{1g}$. The observation of the lower band at 176 cm^{-1} corresponds to the phonon with frequency 174 cm^{-1} having an M_1 symmetry proposed by Belenkii *et al.*[27]

Figure 3 displays the absorption spectra of not purposely doped InSe with the incident light perpendicular to the layer plane, in the spectral range 80–120 cm^{-1}. For E⊥c (curve 1) one band at 103.5 cm^{-1} (line P_1) is observed. This peak has been attributed to the $1s$-$2p_{\pm}$ electronic transition associated to the native donors in InSe.[28] This shallow level at an energy of 12.7 meV has been attributed to interstitial indium atoms,[29] as well as to selenium vacancies.[30] For E∥c, P_1 disappears and the spectrum is dominated by the absorption line of A_1' homopolar optical phonon located at 117 cm^{-1}, that masks other possible lines.

2. In_2Se_3

Figure 4 shows the reflectivity spectra at room temperature of α-In_2Se_3, for polarizations E⊥c (s-polarized light) (curve a) and E∥c (p-polarized light) (curve b). The spectrum recorded in E⊥c polarization (curve a) displays three well-resolved reststrahlen bands in a narrow frequency range. A detailed analysis of the reflectivity spectra of the α phase as a function of the annealing procedure has been published elsewhere.[9,31] At room temperature, the three phonon features are pointed out at 91, 166, and 186 cm^{-1} with a phonon damping factor value lower than 10 cm^{-1}. It has been shown that the post-preparation treatment of the α-In_2Se_3 samples is of prime importance in relation to the defect structure of this material.[9] The increase of the number of defects, i.e., in a quenched sample, affects mainly the electrical conductivity which varies by at least three orders of magnitude. Thus the plasmon contribution appears in the low-frequency region of the far-infrared reflectivity spectrum and phonon-plasmon interactions are observed.

The spectrum recorded in E∥c polarization shown in curve b of Fig. 4 displays only one reststrahlen band at 260 cm^{-1} with a weak oscillator strength. The results of the least-squares fitting are collected in Table III. One can remark on the relative simplicity of the reflectivity spectrum despite the complex structure of this phase. The primitive unit cell of α-In_2Se_3 contains ten atoms forming two layers; there are consequently 27 optical lattice modes at the Brillouin zone center. The infrared spectra, moreover, are dominated by particular modes within each conjugate set. These modes will tend to mask the absorption of their infrared-active conjugate. The mode in each set with all the layers vibrating in phase will tend to control the infrared spectrum.[32] Infrared transmission spectra have been recorded on powdered In_2Se_3 which are consistent with the determination in spectral dependence of $\epsilon_2(\omega)$ for E⊥c. In addition the A_2 vibrational mode is also observed at 257.8 cm^{-1} which is very close to 258.3 cm^{-1} obtained by classical oscillator fitting. From these measurements, we can conclude as follows. First, large anisotropies are found in the phonon frequencies $\omega_{TO}(A_2)>\omega_{TO}(E_1)$. These are compared with anisotropies previously reported[33] for the infrared frequencies of CdI_2-structure crystals and then discussed in terms of force-constant models. Second, the LO-TO splitting is larger for the in-plane mode and final-

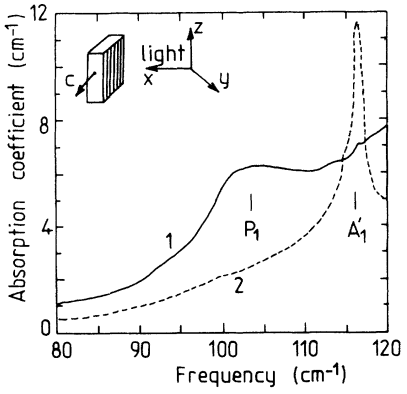

FIG. 3. Absorption coefficient of InSe at 5 K between 80 and 120 cm^{-1} with incident light perpendicular to the layer plane. (1) Light polarized perpendicular to the c axis, (2) light polarized parallel to the c axis.

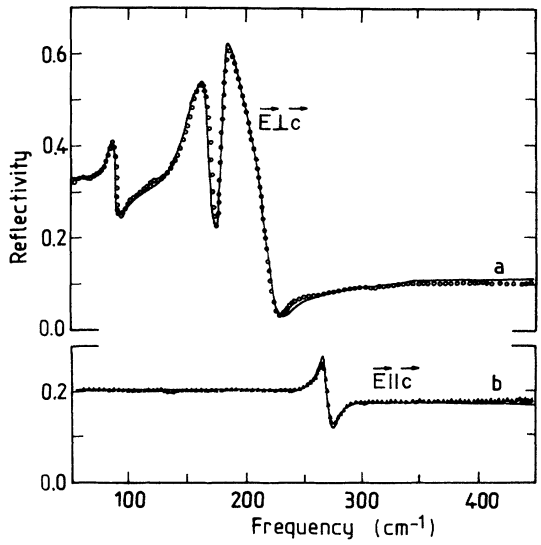

FIG. 4. Far-infrared reflectivity spectra of α-In_2Se_3 single crystal recorded at room temperature with incident light polarization E⊥c (curve a) and E∥c (curve b). Dots are experimental data and full is the best fit using Eq. (3).

TABLE III. Least-squares fitting results.

Symmetry	ω_{TO} (cm^{-1})	ω_{LO} (cm^{-1})	γ (cm^{-1})	S_i	ϵ_∞
$E_1(E\perp c)$	91.2	95	7.4	1.74	9.51
	166.6	179	9.6	8.71	
	186	216	4.6	3.32	
$A_2(E\parallel c)$	258.3	285.5	1.7	0.68	6.37

ly the effective charge is larger for the in-plane mode as well.

Figures 5 and 6 show, respectively, the reflectivity measurements at room temperature and the spectral dependence of both the real and imaginary parts of the dielectric function for the three In_2Se_3 phases: α-In_2Se_3 below the phase transition at 473 K (curve *a*), β-In_2Se_3 at 500 K (curve *b*), and γ-In_2Se_3 (curve *c*). Table IV gives the values of the parameters obtained from the last-squares fit to the measured reflectivity. Below the phase transition the spectrum of α-In_2Se_3 is close to that at room temperature (curve *a* of Fig. 5).

After heating at 200 °C, we get the spectrum of the β phase (curve *b* of Fig. 5) which is characterized by only one phonon feature at $\omega_0 = 164$ cm^{-1} and a damping factor of about 36 cm^{-1}. From the least-squares fitting an infinite dielectric constant of 7.23 is obtained which is the lowest value of the In_2Se_3 phases. The phase transition at 473 K is also found reversible by the FIR measurements with the appearance of a large hysteresis on cooling down the sample. These results confirm the change of crystal symmetry of β phase associated with the reversible distortion of the indium sublattice. The broad reststrahl band observed in the β-phase spectrum can be attributed to the increase of ionicity of this form. According to the crystallographic model of the $\alpha \rightarrow \beta$ phase transition,[34] the indium atom occupies octahedral sites and induces phonons with more polar character. Here we observe an important difference between the two phases from the point of view of vibrational properties which are connected with the change of coordination in the unit cell. Thus, from the sum rule, the value of the term $\epsilon_0 - \epsilon_\infty$ which is the oscillator strength $\Delta\epsilon$ of the mode increases compared with that of the α phase. On the other hand, the damping factor has a high value of 36 cm^{-1} which can also be associated with the temperature dependence of the phonon interactions.[35]

The spectrum of the γ-In_2Se_3 phase (curve *c* of Fig. 5) exhibits four oscillators which are very well resolved in a narrow spectral domain from 180 to 230 cm^{-1}. The results of the analysis listed in Table IV show that the damping factor has a very low value for all oscillators and gives a permittivity value of 11.2 and 8.09 for ϵ_0 and ϵ_∞, respectively. One can remark on the relative simplicity of the reflectivity spectrum despite the complex structure of this phase.

3. In_4Se_3 and $InSe_{1.2}$

Curve *a* of Fig. 7 shows the reflectivity spectrum of In_4Se_3 single crystal recorded at room temperature for $E\perp c$ in the spectral range from 20 to 450 cm^{-1}. The spectrum displays six reststrahlen bands at 40, 73, 97, 158, 196, and 223 cm^{-1}. Considering the reported data on its structure In_4Se_3 has an orthorhombic structure with an elementary cell of 28 atoms[16] and its lattice is characterized by 81 optical normal modes. The vibrational spectrum of In_4Se_3 originates from intralayer and deformation vibrations of the In—Se and Se—Se lattice bonds, but also from interlayer modes which appear at lower frequencies.[36] The energy positions of the band attributed to the In—Se bonds are situated around 178 cm^{-1} which is the transverse optical mode of the In—Se bonds observed in the first-order phonon spectrum of InSe.

Curve *b* of Fig. 7 shows the reflectivity spectrum of $InSe_{1.2}$ single crystal recorded at room temperature for $E\perp c$. This spectrum contains four main reststrahlen bands at 98, 151, 181, and 215 cm^{-1}. $InSe_{1.2}$ has a monoclinic structure with a unit cell formed by 26 atoms. The lattice of $InSe_{1.2}$ is characterized by 75 optical normal modes which cannot be analyzed rigorously because of the lack of information on the force constants. We can only admit that the weak band at 215 cm^{-1} is due to the In—In bonds which are covalent and similar in both In_4Se_3 and $InSe_{1.2}$ structures.[36] The frequencies of the TO

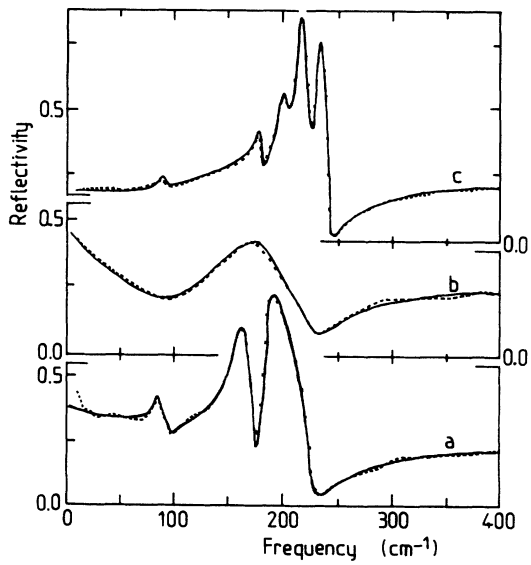

FIG. 5. Far-infrared reflectivity spectra of the different phases: curve *a*, α-; curve *b*, β-; and curve *c*, γ-In_2Se_3 at ambient temperature. These measurements were carried out using a liquid-He cooled detector and a spectral resolution of 2 cm^{-1}.

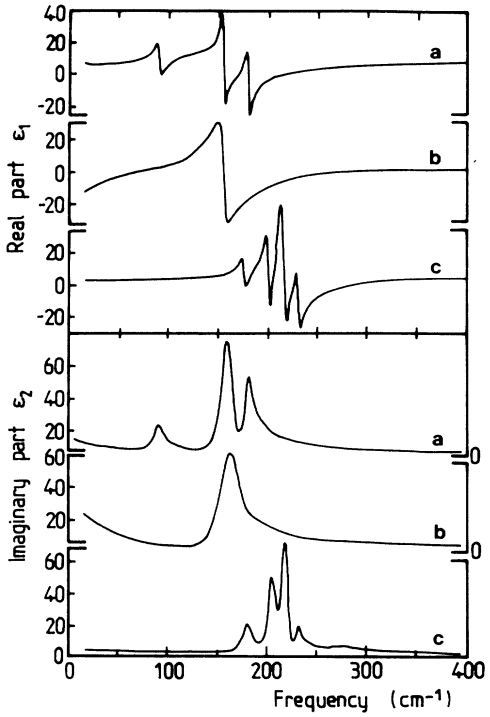

FIG. 6. The spectral dependence of both the real and the imaginary part of the dielectric function of the different phases: curve *a*, α-; curve *b*, β-; and curve *c*, γ-In_2Se_3.

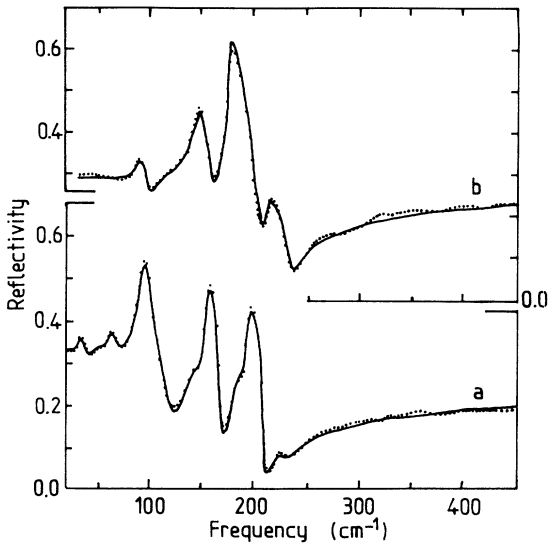

FIG. 7. Curve *a*, far-infrared reflectivity spectrum of In_4Se_3 single crystal recorded at room temperature. Curve *b*, far-infrared reflectivity spectrum of $InSe_{1.2}$ single crystal recorded at room temperature. Dots are experimental data and full line is the best fit using Eq. (3).

and LO phonons of In_4Se_3 and $InSe_{1.2}$ crystals are listed in Table V.

B. Temperature dependence of phonon features

Figure 8 displays the reflectance infrared spectra of InSe at five temperatures for the E$\perp c$ polarization. Other spectra at intermediate temperatures were measured and analyzed, but need not be shown here.

The problem of the frequency shift of one-phonon lines of an anharmonic crystal has been treated by many authors.[37–39] Chang and Mitra[40] have observed that the phonon frequency shifts to lower values as the temperature increases. This is the net result of the two effects, namely, the anharmonic coupling and thermal expansion. This can be expressed as

$$\Omega_i=\omega_i(0)-\Delta\omega_i(T)\ , \tag{7}$$

where $\omega_i(0)$ is the observed TO or LO frequency at $q=0$ and $\Delta\omega_i(T)$ is the temperature-dependent term. In this study, the thermal expansion will be neglected. The second term can be related to a process of phonon-phonon interaction given by

$$\Delta\omega_i(T)=a_i[2n(\Omega_i/2)+1] +b_i[3n^2(\Omega_i/3)+3n(\Omega_i/3)+1]\ , \tag{8}$$

where $n(\Omega_i)=1/[\exp(h\Omega_i/k_BT)]$ is the phonon occupation number evaluated at the average $\Omega_i/2$ for a two-phonon decay and at $\Omega_i/3$ for a three-phonon decay. a_i and b_i are cubic and quartic anharmonic parameters, respectively.

Following the same authors[41–43] a simplified formula deduced from the anharmonic quantum theory[39] has been utilized to fit the temperature dependence of phonon-damping. If only additive phonon-phonon interactions are retained, damping $2\Gamma(T)=\gamma(T)$ for $\omega_i\approx\Omega_i$ may be written in the simple form

$$\Gamma(T)=c_i[2n(\Omega_i/2)+1] +d_i[3n^2(\Omega_i/3)+3n(\Omega_i/3)+1]\ . \tag{9}$$

In view of the results of Table VI, the normal modes of InSe exhibit nearly equal damping for the transverse and the longitudinal vibration at a given temperature in the whole temperature range. Results of the temperature

TABLE IV. Fit to measured reflectivity data.

Phase	β-In_2Se_3			γ-In_2Se_3		
	ω_{0j} (cm^{-1})	γ_j (cm^{-1})	ϵ_∞	ω_{0j} (cm^{-1})	γ_j (cm^{-1})	ϵ_∞
	164	36	7.23	177	7.9	8.09
				201.5	6.5	
				219	4.3	
				235	3.2	

TABLE V. TO and LO phonon frequencies.

Sample	Modes (cm^{-1}) ω_{TO}	ω_{LO}	f_i	ϵ_0	ϵ_∞
In_4Se_3	40	42	0.824	12.51	5.60
	73	76	1.520		
	97	116	3.102		
	158	169	0.867		
	196	209	0.532		
	223	226	0.061		
$InSe_{1.2}$	97	102	2.017	18.23	9.37
	151	160	3.695		
	181	208	2.898		
	215	230	0.250		

dependence of the mode frequency and the phonon damping are listed in Table II. The small discrepancies between LO and TO damping which are found in some cases do not appear to be significant within the experimental error.

The temperature dependence is essentially described by the cubic term.[44] If one defines the effective Debye temperature Θ_i for mode i by $\Theta_i = hc\Omega_i/k_B$, then from the data in Table II for InSe, $\Theta_{LO} = 250$ K. It is at and above the effective Debye temperature that cubic anharmonicity leads to linear temperature dependences of $\Delta\omega_i$ and Γ. The small quartic contributions added to improve the fits for the TO mode are not very significant in view of the experimental uncertainty. The ratio $b_i/a_i\Omega_i$ always keeps a low level, typically equal to 2×10^{-4} cm. This quartic contribution, if it actually exists, remains much lower than the cubic one even at room temperature. A qualitative argument has been given by Gurevich and Ipatova[43] for the understanding of the magnitude of the ratio b_i/a_i. They consider that the greater the separation between phonon branches, the more difficult it is to satisfy the conservation laws which enter into the cubic contribution to the damping whereas the quartic contribution is much less sensitive to the branch separation.

C. Doped layered materials

Figure 9 shows the FIR spectrum of a sulfur-doped In_2Se_3 crystal recorded at room temperature for $E \perp c$. Samples of $In_2Se_{2.9}S_{0.1}$ have been prepared by sulfur transport at 140° C for two days.[8] The FIR reflectivity measurements exhibit three different features: (i) the three reststrahlen bands at 92, 166, and 188 cm^{-1} which are those observed for pure In_2Se_3; (ii) three additional weak bands at 220, 265, and 300 cm^{-1}; and (iii) an increase of the background at lower frequency.

The high-frequency bands characterize the mixed character of this compound; the reflectivity spectrum of the solid solution maintains the general features of the host material but we observe modes which originate from a fractional amount of In_2S_3 in the mixed compound. Infrared reflectivity of α-In_2Se_3 presents five main bands at 200, 227, 263, 313, and 358 cm^{-1}. The incorporation of S atoms in In_2Se_3 gives three local modes lying higher in frequency that the LO-mode frequencies of pure In_2Se_3. The oscillator strength of these peaks is very weak ($f_i < 0.1$) and the ratio $\epsilon_0/\epsilon_\infty$ remains constant at a value of 1.74. It is known that the alloys have mainly the same crystal structure as the parent crystal, however, the distribution of the constituent ions over the sublattices is not known but we observed a small increase of the disordering after the substitution of S-Se atoms in the mixed crystals. The increase of the low-frequency reflectivity can be interpreted as an increase of the free-carrier concentration in the layers.[45]

Figure 10 shows the far-infrared spectra of four doped-InSe single crystals. Doping agents, namely, Zn, Sn, GaS, and InS were added to the polycrystalline powder used in the Bridgman method. Investigations on the electrical transport properties of these samples have been reported elsewhere.[29,46] These spectra exhibit at least three features: (i) the strong reststrahlen band which appears at the same frequency as that for pure InSe, (ii) a small free-carrier contribution at low frequency for the sulfur-doped samples and (iii) six new peaks which can be identified at 280, 305, 340, 400, 440, and 485 cm^{-1}. They are observed in all the samples. The frequency values of these peaks are in good agreement with those reported previously.[27,46,47] They are attributed to phonon combination modes using Γ-point phonons.

Introduction of impurities or point defects in the InSe crystal lattice destroys the translational invariance of the crystal and results mainly in two effects on the lattice normal modes:[48] a perturbation of the normal modes specific to the introduced impurity and a polarization induced on the normal modes independent of the nature of

TABLE VI. TO and LO mode parameters.

Mode	Parameters in cm^{-1} ω_{0j}	a_i	b_i	c_i	d_i
TO	179	−0.28	−0.005	0.80	0.028
LO	218	−0.97		1.20	

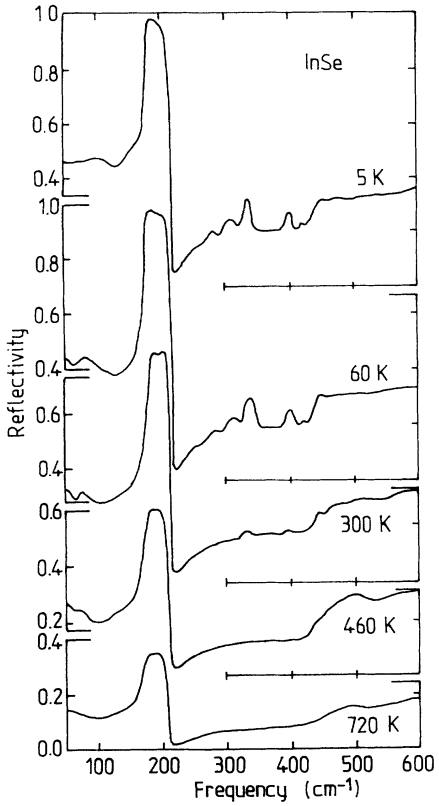

FIG. 8. Far-infrared reflectivity spectra of InSe single crystal recorded at different temperatures: curve *a*, 5; curve *b*, 60; curve *c*, 300; curve *d*, 460; and curve *e*, 720 K.

the impurity. These last effects make optically active lattice normal modes which are otherwise inactive such as the low-frequency combination $E_{2u}+E_{1g}$ mode observed at 76 cm^{-1}. This mode has been calculated to be a silent mode by Riede *et al.*[46] using the linear chain model developed by Wieting.[49] A second consequence of the impurities or induced disorder can be the enhancement of high-frequency two-phonon combination modes as it is observed in Fig. 10.

Far-infrared reflectivity measurements corroborate that the problem of impurity levels in layered semiconductors may be more complex than in three-dimensional

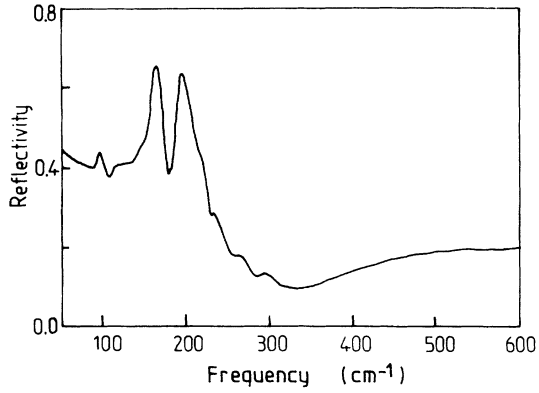

FIG. 9. Far-infrared reflectivity spectrum of S-doped In_2Se_3 single crystal.

bonded crystals. Even at a concentration of dopant, with 0.3 at. % Sn, for instance (curve *c*), we observe the weak appearance of free-carrier contribution, i.e., a plasma edge in the reflectivity spectrum. Only for indium-sulfide-doped InSe (curve *a*) does a strong plasmon contribution appear at low frequency. Using a simple Drude model free-carrier densities, n_{opt}, are calculated and a large plasmon damping factor of about 100 cm^{-1} is found. Calculated values of the parameters are listed in Table VII.

D. Lithium-intercalated In_2Se_3

Lithium-intercalated In_2Se_3 single crystals have been prepared by chemical reaction in *n*-butyl lithium (*n*-BuLi). Samples are immersed for 6 into 0.4*M* solution of *n*-BuLi dissolved in hexane.[4] Pristine material has a conductivity of 0.01 $\Omega^{-1}cm^{-1}$ and Hall-effect measurement show concentration of *n*-type carriers of 1×10^{16} cm^{-3} and mobility of 6.2 $cm^2V^{-1}s^{-1}$ at room temperature. Figure 11 shows the reflectivity spectra recorded at different temperatures from 5 to 300 K. Other spectra at intermediate temperatures were measured and analyzed, but shall not be shown here. In these curves, dots represent experimental points at one wave number. The full line is a theoretical fit, the parameters of which are given below.

In order to reduce the weakness of the classical dispersion theory, a convenient model consists of utilizing the factorized form of the dielectric function[50–52]

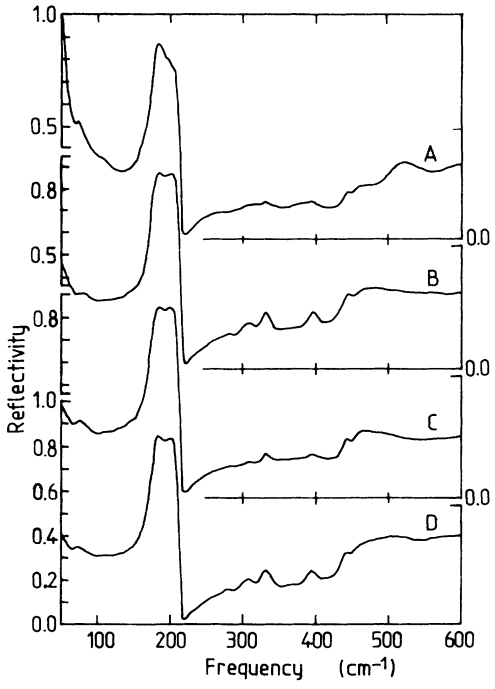

FIG. 10. Far-infrared reflectivity spectra of doped-InSe single crystals: curve *a*, 0.015 at. % InS doped; curve *b*, 0.01 at. % GaS doped; curve *c*, 0.3 at. % Sn doped; and curve *d*, 0.1 at. % Zn doped. These spectra are recorded at room temperature for E⊥*c*.

TABLE VII. Parameters calculated using a simple Drude model.

Sample	Dopant	Concentration of dopant (ppm)	ω_p (cm^{-1})	Carrier density n_{opt} (cm^{-3})
A	InS	150	122	1.4×10^{17}
B	GaS	100	72	4.9×10^{16}
C	Sn	3000	35	1.2×10^{16}
D	Zn	1000	22	4.1×10^{15}

$$\epsilon(\omega)=\epsilon_\infty \prod_{j,\mathrm{ph}} (\omega_{\mathrm{LO},j}^2-\omega^2\pm i\gamma_{\mathrm{LO},j}\omega) \times(\omega_{\mathrm{TO},j}^2-\omega^2\pm i\gamma_{\mathrm{TO},j}\omega)^{-1} , \quad (10)$$

that describes LO modes more correctly when their damping differs. The LO dampings are even stronger than from those of TO modes. Since the reducing treatment affects the LO modes much more than the TO modes and since the plasmon which is expected owing to the carrier concentration is also a longitudinal excitation, it is clear that the spectrum is characteristic of LO phonon-plasmon coupling. The model of Eq. (10) is adequate to describe a plasmon alone by setting $\omega_{\mathrm{TO}}=0$, so that Eq. (10) reduces to

$$\epsilon_{pl}=\epsilon_\infty(\omega_p^2-\omega^2\pm i\gamma_p\omega)[\omega(-\omega\pm i\gamma_0)]^{-1} , \quad (11)$$

$$\epsilon_{pl}=\epsilon_\infty[1-\{\omega_p^2\pm i\omega(\gamma_p-\gamma_0)\}\{\omega(\omega\pm i\gamma_0)\}^{-1}] , \quad (12)$$

where ω_p is the plasma frequency, γ_p the plasmon damping and γ_0 the damping at zero frequency which may be different from γ_p and this may be an improvement with respect to the Drude formula if the plasmon damping is considered as a function instead of a constant although an assumption is made about the form of the plasmon damping function.[52] Equation (12) reduces to the Drude formula when $\gamma_p=\gamma_0$. With the precaution of setting one of the TO frequencies equal to zero in Eq. (12), this dielectric function model is able to describe the reflectivity spectrum of a system of plasmon-phonon coupled modes correctly when several phonon modes are strongly polar, that is, when the reflectivity bands are wide.

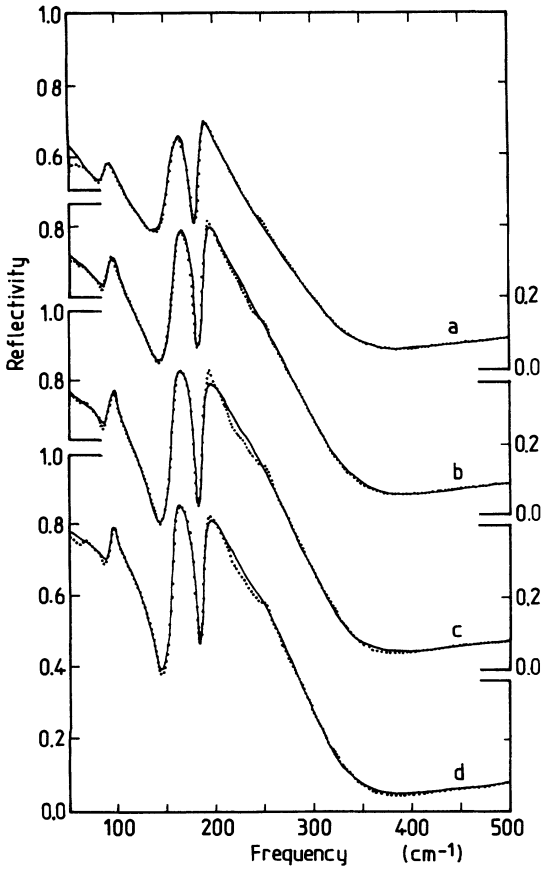

FIG. 11. Far-infrared reflectivity spectra of Li-intercalated In_2Se_3 single crystals at different temperatures; curve *a*, 300 K; curve *b*, 180 K; curve *c*, 100 K; and curve *d*, 5 K. In these curves, dots represent experimental points at one wave number and the full line is a theoretical fit using Eq. (13). We should note that in the high-energy side the reflectivity decreases almost linearly.

It is of interest to obtain the oscillator parameters of the pure-phonon and the pure-plasmon excitations. To this end, we decompose Eq. (10) into a sum of two contributions. The pure-lattice dielectric function is still given by Eq. (10) which has the advantage of describing the pure-phonon reflectivity correctly. The second contribution is consistently given by Eq. (12) minus a quantity ϵ_∞ which is already incorporated into the lattice term. Equation (10) is thus rewritten

$$\epsilon(\omega)=\epsilon_\infty \left[\prod_{j,\mathrm{ph}}(\omega_{\mathrm{LO},j}^2-\omega^2\pm i\gamma_{\mathrm{LO},j}\omega) \times(\omega_{\mathrm{TO},j}^2-\omega^2\pm i\gamma_{\mathrm{TO},j}\omega)^{-1} -\{\omega_p^2\pm i\omega(\gamma_p-\gamma_0)\}\{\omega(\omega\pm i\gamma_0)\}^{-1}\right] . \quad (13)$$

Both Eqs. (3) and (13) are strictly equivalent for an appropriate choice of parameters. Equation (13) allows the same fitting to the data as Eq. (3) does, but while TO excitation parameters are the same in both formulas, the LO parameters now correspond to the pure phonons and the plasmon. In other words, whereas the $\omega_{\mathrm{TO},j}$'s and zero are poles of the dielectric function in both equations [Eqs. (3) and (13)], the $\omega_{\mathrm{LO},j}$'s are the zeros of $\epsilon(\omega)$ and consequently the poles of the energy-loss function $\eta(\omega)=1/\epsilon(\omega)$ in Eq. (3) and this is no longer the case in Eq. (13).

Let us first consider the temperature dependence of the lattice term for the spectra of Fig. 11. The qualitative features of these spectra are readily apparent: (i) the

phonon-mode spectrum which has been discussed above for pure In_2Se_3 (Fig. 4) appears to be temperature dependent, and (ii) the free-carrier contribution due to the lithium insertion into the van der Waals gap of the layered structure and the charge transfer occurring between the guest species and the host structure.[53]

Values of the imaginary part of the inverse dielectric function, the energy-loss function, $\mathrm{Im}(-\epsilon^{-1})=\epsilon_2/(\epsilon_1^2+\epsilon_2^2)$, and the imaginary part of the dielectric function ϵ_2 derived from reflectivity curves have been calculated in the range 5–300 K. Maxima of ϵ_2 correspond to the frequency of transverse (dissipative) oscillators. The crystal TO frequencies are thus visible as strong peaks in ϵ_2 at $\Omega_i=\omega_i/2\pi c$ and the free-carrier contribution appears in the low-frequency region where the absorption has a very large value. The temperature variation of the position of these TO modes is plotted against temperature in Fig. 12. We may note that the lower and higher phonons are temperature dependent whereas the TO_2 mode is nearly temperature independent.

Maxima of the $\mathrm{Im}(-\epsilon^{-1})$ curve are connected with oscillators having longitudinal polarization character. Four maxima corresponding to Ω_+ and Ω_- plasmon-phonon coupled modes are observed.[54,55] The strongest peak situated at high energy has the plasmon dominant character. Its intensity increases with the decreasing temperature. The oscillator strength is derived from the $\epsilon_2(\omega)$ curves by the usual formula

$$f_i=\frac{2}{\pi}\int_{\text{peak}}\epsilon_2(\omega)\omega^{-1}d\omega \ . \tag{14}$$

f_2 and f_3, the oscillator strengths of the fundamental TO_2 and TO_3 phonons, are practically temperature independent. Conversely, the oscillator strength of the high-frequency fundamental mode TO_1, f_1, is strongly temperature dependent. All these parameters were evaluated from the experimental curves and are plotted in Fig. 13.

Using the factorized form of the Lyddane-Sachs-Teller equation,[24]

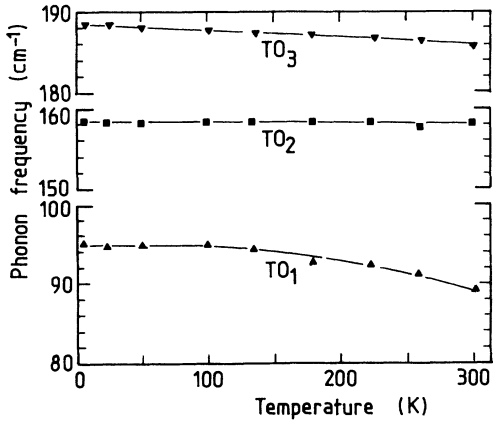

FIG. 12. Temperature dependence of the transverse phonon-mode frequencies for Li-intercalated In_2Se_3 single crystal.

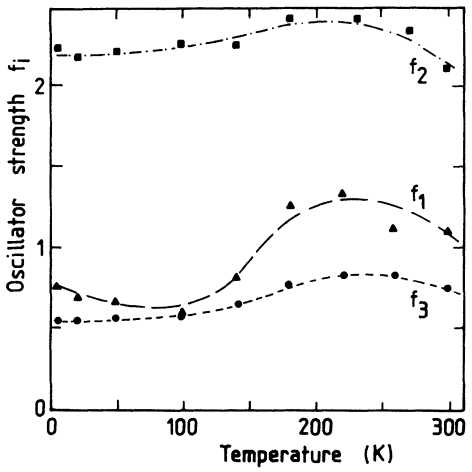

FIG. 13. Temperature dependence of oscillator strength for Li-intercalated In_2Se_3 single crystal.

$$\epsilon_0=\epsilon_\infty\prod_j(\omega_{\mathrm{LO},j}/\omega_{\mathrm{TO},j})^2 \ , \tag{15}$$

the high-frequency dielectric constant ϵ_∞ can be estimated. One should note that for a finite-gap semiconductor, ϵ_∞ can be given directly by reflectivity curves for $\omega\gg\omega_{\mathrm{TO}}$,

$$\epsilon_\infty=\{[1+(R_\infty)^{1/2}][1-(R_\infty)^{1/2}]\}^2 \ . \tag{16}$$

Figure 14 shows the temperature dependent of ϵ_∞ as a parameter in Eq. (13) to fit with experimental reflectivity. Variations of ϵ_∞ strongly influence the form and position of the high-energy reflectivity minimum, especially at low temperatures, and the absolute value of reflectivity on the high-energy side. ϵ_∞ is therefore determined with a computational uncertainty of ± 0.2.

Now let us consider the free-carrier contribution to the reflectivity spectra of Fig. 11. These spectra exhibit a high reflectivity factor on the low-energy side and on the high-energy side the reflectivity diminishes almost linearly with the frequency. In a simple model with one LO and one TO frequency, one expects two singularities[54,55] as two maxima of the function $\mathrm{Im}(-\epsilon^{-1})$ representing longitudinal modes. The frequencies generally labeled Ω_+ and Ω_- correspond to longitudinal oscillations with the lattice and electron plasma vibrating, respectively, in

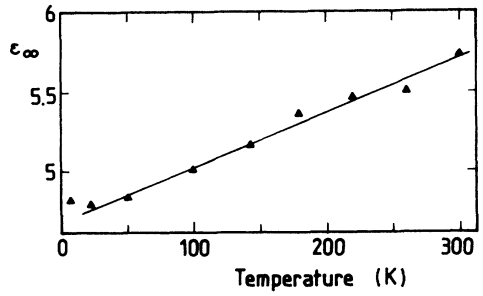

FIG. 14. Temperature dependence of ϵ_∞ as a parameter in Eq. (13) for Li-intercalated In_2Se_3 single crystal.

phase and 180° out of phase.[56] In In_2Se_3 the situation is more complex. Because of its three fundamental modes, it is necessary to include other oscillators. The plasma frequency is temperature independent and has a value of 300 cm^{-1}.

We observe a weak variation in the plasma frequency over the entire temperature range 5–300 K. This is in good agreement with the Hall-effect measurements.[53] The sample immersed into n-type BuLi for shorter periods of time (6 h) and then left to equilibrate during two weeks has concentration of n-type carriers of 2.3×10^{18} cm^{-3} and Hall mobility of 109.9 $cm^2V^{-1}s^{-1}$. Upon lithium insertion it exhibits an increase of conductivity up to 40.4 $\Omega^{-1}cm^{-1}$ at room temperature.

A good fit to optical data is achieved by making a distinction between the damping γ_p at the plasma frequency and the "static" damping γ_0.[57] This is an improvement with respect to the Drude formula, which is nothing else than Eq. (12) with the restriction $\gamma_p=\gamma_0$. Then the scattering rate is written in the form

$$1/\tau(T,\omega)=\gamma(T,\omega)=\gamma_0+(\gamma_p-\gamma_0)\omega^2/\omega_p^2 . \quad (17)$$

The surprisingly good representation of the reflectivity data with the ω^2 frequency variation of the damping provides evidence for electron-electron scattering in the range 20–1000 cm^{-1}. Figure 15 shows the temperature dependence of the damping γ_p and the static damping γ_0. As expected the plasma damping is nearly temperature independent. This is in good agreement with the Hall-effect measurements.[53] The static damping γ_0 can be expressed in the form[58]

$$\gamma_0(T)=AT^{\beta}+B , \quad (18)$$

where B is the value of the static damping at zero temperature and A a constant. From the fit of Fig. 15 the exponent β has a value of 1.9 ± 0.1 which is close to a quadratic temperature dependence of the static damping γ_0. This T^2 dependence of the relaxation rate is related to the electron-electron scattering which appears to be the mechanism for the conduction in Li-intercalated In_2Se_3.

It is interesting to compare both sets of experimental

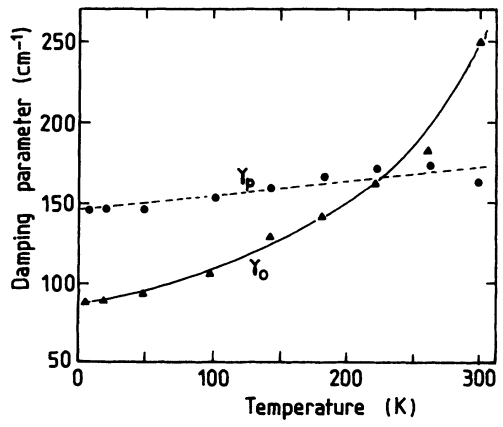

FIG. 15. Temperature dependence of the plasma damping γ_p and the static damping γ_0 given the scattering rate of Eq. (17) for Li-intercalated In_2Se_3 single crystal.

TABLE VIII. Reflectivity and dc transport data.

Measurement	dc transport	Optical reflectivity
Carrier concentration $N_{H,\omega}$ (cm^{-3})	2.3×10^{18}	1.97×10^{18}
Mobility $\mu_{H,\omega}$ ($cm^2V^{-1}s^{-1}$)	109.9	183
dc conductivity σ_0 ($\Omega^{-1}cm^{-1}$)	40.4	58.2

data, i.e., the Hall transport measurements and infrared reflectivity spectroscopy reported in Table VIII. We observe the appearance of a plasma edge at 300 cm^{-1} above the reststrahlen region. A decrease of R_∞ is observed. Using Eq. (13) with the plasmon damping γ_p, we obtain an optical mobility μ_ω of 183 $cm^2V^{-1}s^{-1}$ which is comparable to the value of 109.9 $cm^2V^{-1}s^{-1}$ measured by Hall effect.[53] If we admit that the carrier concentrations obtained by the two methods have the same value, the effective mass m^* of the Li-intercalated sample is given by

$$m^*=4\pi e(\omega_p^2\epsilon_\infty R_H)^{-1} . \quad (19)$$

The result shows that free-carrier effective mass is $m^*=0.3m_0$, for an n-BuLi sample intercalated for 6 h. We can remark that the variations in the plasma damping are also compatible with the decrease of the mobility. It is interesting to estimate the dc conductivity from optical reflectivity measurements

$$\sigma_0=\omega_p^2\epsilon_\infty\tau . \quad (20)$$

We obtain a value of 58.2 $\Omega^{-1}cm^{-1}$ which is close to 40.4 $\Omega^{-1}cm^{-1}$, the dc transport measurement at room temperature.

IV. CONCLUSION

This work reports far-infrared reflectivity spectra of different indium selenides, i.e., InSe, In_2Se_3, In_4Se_3, and $InSe_{1.2}$. $E\|c$ and $E\perp c$ polarization spectra of InSe and In_2Se_3 have been recorded and analyzed using a factorized form of the dielectric function. The $E\|c$ polarization spectrum of In_2Se_3 single crystal has been studied. Vibrational spectra of In_4Se_3 and $InSe_{1.2}$ have bene analyzed using Kramers-Kronig relationship.

We can remark (i) the effect of the anisotropy on the effective charge in InSe, (ii) the effective charge for the in-plane mode is higher than that along the c axis, and (iii) the ratio $e_T^*(\perp)/e_T^*(\|)$ is 5.53 in InSe. This may be taken as evidence for the strongest ionicity in InSe.

This work provides a clear identification of the temperature dependence of the lattice modes of InSe single crystal. Until now, the layered materials of the III-VI family have not yet been investigated in the whole temperature range from 5 to 720 K. We show that in this range, the temperature dependence of the frequency and damping of phonon are essentially described by the cubic term in an anharmonic model. It is at and above the effective Debye temperature, $\Theta_{LO}=250$ K, that cubic anharmonicity leads to linear temperature dependences of $\Delta\omega_i$ and Γ.

The small quartic contributions are not very significant in view of the experimental uncertainty. We can attribute the weak ratio between the quartic and the cubic term as the consequence of the separation between phonon branches in order to satisfy the conserving laws which enter into the cubic contribution to the phonon damping.

Far-infrared spectra of doped layered materials have also been investigated. In_2Se_3 doped with 10% sulfur exhibits a superposition of the spectra of In_2Se_3 and α-In_2S_3. Introduction of impurities and disorder in the crystal lattice of InSe enhances the second-order infrared-active spectrum and shows the strong appearance of the low-frequency phonon combination. The free-carrier contribution of the dielectric function has also been observed.

Finally we have studied the far-infrared reflectivity of Li-intercalated In_2Se_3 as a function of the temperature. The qualitative features of the temperature dependence of the reflectivity spectra are readily apparent: (i) the phonon-mode spectrum which has been discussed above for pure In_2Se_3 appears to be temperature dependent, and (ii) the free-carrier contribution due to the lithium insertion into the van der Waals gap of the layered structure and the charge transfer occurring between the guest species and the host structure. We may note that the lower and higher phonons are temperature dependent whereas the TO_2 mode is nearly temperature independent. This behavior is reflected by the oscillator strength determination of the different modes. The free-carrier contribution to the reflectivity spectra of Li-intercalated In_2Se_3 is represented by the singularities in the energy-loss function.

A good fit to optical data is achieved by making a distinction between the damping γ_p at the plasma frequency and the "static" damping γ_0. The surprisingly good representation of the reflectivity data with the ω^2 frequency variation of the damping provides evidence for electron-electron scattering in the range 20–1000 cm^{-1}. The T^2 dependence of the relaxation rate is also related to the electron-electron scattering which appears to be the mechanism for the conduction in Li-intercalated In_2Se_3.

ACKNOWLEDGMENTS

The authors wish to thank Professor J. L. Birman and Professor R. F. Wallis for valuable comments concerning the contents of this paper. Numerical calculations have been performed with the aid of an infrared analysis data software written by Dr. D. Massiot and Dr. F. Gervais (from CNRS-CRPHT, Orlèans France) who are gratefully acknowledged. Laboratoire de Physique des Solides is Laboratoire associé au CNRS No. 154. Laboratoire de Physique des Milieux Condensés is Laboratoire Associé au CNRS No. 782.

[1]W. Y. Liang, in *Intercalation in Layered Materials,* Vol. 148 of *NATO Advanced Study Institute, Series B: Physics,* edited by M. S. Dresselhaus (Plenum, New York, 1986), p. 31.
[2]J. A. Wilson and A. D. Yoffe, Adv. Phys. **18**, 193 (1969).
[3]A. Segura, J. P. Guesdon, J. M. Besson, and A. Chevy, J. Appl. Phys. **54**, 876 (1983).
[4]C. Julien and I. Samaras, Solid State Ionics **27**, 101 (1988).
[5]G. K. Slavnova and A. A. Eliseev, Russ. J. Inorg. Chem. **8**, 861 (1963).
[6]A. Likforman and M. Guittard, C. R. Acad, Sci., Ser. C **279**, 33 (1974).
[7]C. Julien, A. Chevy, and D. Siapkas, Phys. Status Solidi A **118**, 553 (1990).
[8]J. Fotsing, C. Julien, M. Balkanski, and K. Kambas, Mater. Sci. Eng. B **1**, 139 (1988).
[9]I. Lelidis, D. Siakpas, C. Julien, and M. Balkanski, Mater. Sci. Eng. B **3**, 133 (1989).
[10]V. P. Savchin, Fiz. Tekh. Poluprovodn. **15**, 1430 (1981) [Sov. Phys. Semicond. **15**, 827 (1981)].
[11]S. Mori, J. Phys. Soc. Jpn. **35**, 310 (1973).
[12]A. Chevy, J. Cryst. Growth **51**, 157 (1981).
[13]A. Likforman, D. Carre, J. Etienne, and B. Bachet, Acta Crysallogr., Sect. B **31**, 1252 (1975).
[14]M. Jouanne, C. Julien, and M. Balkanski, Phys. Status Solidi B **144**, K147 (1987).
[15]A. Likforman, D. Carré, and R. Hillel, Acta Crystallogr., Sect. B **24**, 1 (1978).
[16]J. H. C. Hogg, H. H. Sutherland, and D. J. Williams, Acta Crystallogr., Sect. B **29**, 15 (1973).
[17]A. Likforman, D. Messin, M. Guittard, and J. Flahaut, C. R. Acad. Sci., Ser. C **274**, 378 (1972).
[18]J. H. C. Hogg, Acta Crystallogr., Sect. B **27**, 1630 (1971).
[19]S. Nakashima, M. Hangyo, and A. Mitsuishi, in *Vibrational Spectra and Structures,* edited by J. R. Durig (Elsevier, Amsterdam, 1985), Vol. 14, p. 305.
[20]F. Gervais, in *Infrared and Millimeter Waves,* edited by K. J. Button (Academic, New York, 1983), Vol. 8, p. 279.
[21]N. M. Gasanly, B. M. Yvadov, V. I. Tagirov, and E. A. Vinogradov, Phys. Status Solidi B **89**, K43 (1978).
[22]K. R. Allakhverdiev, S. S. Babaev, E. Y. Salaev, and M. M. Tagyev, Phys. Status Solidi B **96**, 177 (1979).
[23]S. Jandl, M. Banville, and J. Deslandes, Can. J. Phys. **59**, 198 (1981).
[24]R. H. Lyddane, R. G. Sachs, and E. Teller, Phys. Rev. **59**, 673 (1941).
[25]M. Balkanski, in *Optical Properties of Solids,* edited by F. Abelès (North-Holland, Amsterdam, 1972), p. 526.
[26]G. Lucovsky, R. M. White, J. A. Benda, and J. F. Revelli, Phys. Rev. B **7**, 3859 (1973).
[27]G. L. Belenkii, L. N. Alieva, R. K. Nani, and E. Y. Salaev, Phys. Status Solidi B **82**, 705 (1977).
[28]E. Kress-Rogers, G. F. Hoppert, R. J. Nicholas, W. Hayes, J. C. Portal, and A. Chevy, J. Phys. C **16**, 4285 (1983).
[29]A. Segura, K. Wunstel, and A. Chevy, Appl. Phys. A **31**, 139 (1983).
[30]T. Ikari, S. Shigetomi, Y. Koga, and S. Shigetomi, Phys. Status Solidi B **103**, K81 (1981).
[31]I. Lelidis, D. Siapkas, C. Julien, and M. Balkanski, in *Phonons 89,* edited by S. Hunklinger, W. Ludwig, and G. Weiss (World Scientific, Singapore, 1990), p. 1162.
[32]T. J. Wieting and J. L. Verble, in *Electrons and Phonos in Layered Crystal Structures,* edited by T. J. Wieting and M. Schlüter (Reidel, Dordrecht, 1979), p. 321.
[33]G. Lucovsky and R. M. White, Nuovo Cimento B **38**, 290 (1977).
[34]K. Osamura, Y. Murakami, and Y. Tomiie, J. Phys. Soc. Jpn.

21, 1848 (1966).
[35]K. D. Möller and W. G. Rothchild, *Far-Infrared Spectroscopy* (Wiley-Interscience, New York, 1971), p. 460.
[36]V. P. Zakharov, V. P. Savchin, I. M. Stakhira, and G. P. Sheremet, Fiz. Tverd. Tela (Leningrad) **23**, 1881 (1981) [Sov. Phys. Solid State **23**, 1101 (1981)].
[37]A. A. Maradudin and A. E. Fein, Phys. Rev. **128**, 2589 (1962).
[38]V. V. Mitskevich, Fiz. Tverd. Tela (Leningrad) **4**, 3035 (1963) [Sov. Phys. Solid State **4**, 2224 (1963)].
[39]R. F. Wallis, I. P. Ipatova, and A. A. Maradudin, Fiz. Tverd. Tela (Leningrad) **8**, 1064 (1966) [Sov. Phys. Solid State **8**, 850 (1966)].
[40]I. F. Chang and S. S. Mitra, Phys. Rev. B **5**, 4094 (1972).
[41]P. G. Klemens, Phys. Rev. **148**, 845 (1966).
[42]T. Sukurai and T. Sato, Phys. Rev. **4**, 583 (1971).
[43]L. E. Gurevich and I. P. Ipatova, Zh. Eksp. Teor. Fiz. **45**, 231 (1963) [Sov. Phys. JETP **18**, 162 (1964)].
[44]M. Balkanski, R. F. Wallis, and E. Haro, Phys. Rev. B **28**, 1928 (1983).
[45]A. Segura, F. Pomer, A. Cantarero, W. Krause, and A. Chevy, Phys. Rev. **29**, 5708 (1984).
[46]V. Riede, H. Neumann, F. Levy, and H. Sobotta, Phys. Status Solidi B **109**, 275 (1982).
[47]K. Kumazaki and K. Imai, Phys. Status Solidi **149**, K183 (1988).
[48]M. Balkanski, in *Handbook on Semiconductors,* edited by T. S. Moss (North-Holland, Amsterdam, 1980), Vol. 2, p. 497.
[49]T. J. Wieting, Solid State Commun. **19**, 931 (1973).
[50]D. W. Berreman and F. C. Unterwald, Phys. Rev. **174**, 791 (1968).
[51]W. G. Spitzer and D. A. Kleinmann, Phys. Rev. **121**, 1324 (1961).
[52]F. Gervais and J. F. Baumard, Solid State Commun. **21**, 861 (1977).
[53]C. Julien, L. El-Farh, and M. Balkanski, Mater. Sci. Eng. B **7**, 523 (1990).
[54]A. Mooradian and G. B. Wright, Phys. Rev. Lett. **16**, 999 (1966).
[55]B. B. Varga, Phys. Rev. **137**, A1896 (1965).
[56]E. Burstein, in *Elementary Excitations in Solids,* edited by A. A. Maradudin and G. F. Nardelli (Plenum, New York, 1969), p. 367.
[57]J. F. Baumard and F. Gervais, Phys. Rev. B **15**, 2316 (1977).
[58]R. N. Gurzhi, Zh. Eksp. Teor. Fiz. **35**, 965 (1959) [Sov. Phys. JETP **8**, 673 (1959)].